PCCP

PAPER

View Article Online
View Journal | View Issue



Cite this: *Phys. Chem. Chem. Phys.*, 2026, **28**, 6999

# Unraveling the magnetoelectric effect using electric field-controlled magnetic anisotropy: a theoretical study

Flaurent Heully-Alary,[a] Barthélémy Pradines,[a] Benjamin Cahier,[a] Nicolas Suaud,[a] Talal Mallah[b] and Nathalie Guihéry*[a]

This article highlights the microscopic origin of the magnetoelectric effect, which could enable crucial control of magnetic properties using electric fields. In particular, it explains the influence of electric fields on the magnetic anisotropy of a Ni(II) complex characterized by significant uniaxial anisotropy and notable rhombicity. Our findings reveal that the electric field's effect on the axial anisotropy parameter primarily arises from atomic displacements, whereas for the rhombic parameter, it is driven by electronic structure changes. While recent observations show that electric fields applied in the direction of the molecular dipole moment induce a greater variation in $D$ than fields applied perpendicular to it due to greater atomic displacement, here we demonstrate a striking exception: applying the electric field in the molecular direction associated with an almost zero dipole moment causes a variation in $D$ seven times greater than that induced in the direction of a large permanent dipole moment (~10 Debye). This observation reveals a previously unknown magnetoelectric coupling mechanism. We demonstrate that the magnetoelectric effect inducing variations of the zero-field splitting parameters is dictated by the nature of electronic excitations involved in the spin–orbit couplings that produce the magnetic anisotropy, more specifically in the orientation of the orbitals involved in these excitations, rather than by the dipole moment's magnitude. However, as the variation of $D$ is essentially governed by the impact of field-induced geometric changes on the energy of the orbitals involved in these excitations, one may expect larger responses if one of these orbitals points in the direction of the dipole moment. Besides, as this behavior can be rationalized using crystal field theory, it offers a general principle that can help the design of molecules with predictable magnetoelectric responses.

Received 25th August 2025,
Accepted 9th February 2026

DOI: 10.1039/d5cp03260a

rsc.li/pccp



## Introduction

Electric fields hold significant promise as efficient external stimuli for tuning the physical properties of magnetic molecules and materials[1] *via* the magnetoelectric (ME) effect.[2–7] In the context of quantum information, electric fields were initially proposed to perform logical operations on individual atomic spins. This stems from their ability to be more easily focused at the nanoscale than magnetic fields, allowing them to affect electron wave functions and modulate hyperfine interactions.[8]

The strength of the ME response depends on the specific magnetic property under consideration—such as magnetic anisotropy,[9] **g**-tensor,[10–13] hyperfine coupling[14] and exchange interactions.[4,15,16] Notably, electric field tuning of local magnetic anisotropy, *i.e.*, zero-field splitting (ZFS) parameters, enables coherent spin control. This has been demonstrated in both atoms embedded in solid-state environments[17–21] and in molecular systems.[4,5,22]

Theoretical calculations have allowed the description of how electric fields influence the spin Hamiltonian parameters of molecular systems, including interactions like magnetic exchange, anisotropy of exchange tensor and the Dzyaloshinskii–Moriya vector for which the impact of the electric field has not yet been measured.[23–31] However, *ab initio* calculations remain scarce. A deep understanding of the microscopic mechanisms underpinning electric field effects on spin degrees of freedom ultimately requires an analysis of low energy spectrum and wave functions. Since spin is inherently insensitive to electric fields, it must couple with orbital degrees of freedom for the ME effect to occur.

We recently reported such a study[22] on a series of Mn(II) complexes isostructural to the Ni(II) complex studied here,

[a] *Université de Toulouse, CNRS UMR5626, LCPQ, 118 route de Narbonne, F-31062 Toulouse, France. E-mail: nathalie.guihery@irsamc.ups-tlse.fr*
[b] *Institut de Chimie Moléculaire et des Matériaux d'Orsay CNRS, Université Paris-Saclay UMR 8182, 17, avenue des Sciences, Orsay, 91400, France*

using pulsed electron paramagnetic resonance (EPR) spectroscopy and coherent control of superposed quantum states. We showed that the ME effect—reflected in changes in the axial ZFS parameter—can be understood through the analysis of spin–orbit coupled wave functions that explain the contributions of the various excited states to ZFS. The primary conclusion was that the electric field modifies the axial ZFS parameter mainly by altering the molecular geometry, rather than directly affecting the electronic structure. Importantly, applying the electric field perpendicular to the bond associated with the largest dipole moment neither influenced the axial magnetic anisotropy nor introduced any detectable rhombic anisotropy, leading to the conclusion that in the case of Mn(II) complexes the electric field has little effect on ZFS if applied along a direction with a weak dipole moment. These findings align with previous results on Mn(II) and Fe(III) ions (both $d^5$ ions with weak spin–orbit coupling) embedded in piezoelectric matrices, where electric fields modulate the local charge environment and amplify ME effects.[17,18,20] However, due to the inherently weak ME coupling in such $d^5$ systems that EPR can detect, it is difficult to deconvolute individual mechanisms and fully elucidate the microscopic origin of ME.

The main goal of this study is to elucidate the mechanism by which electric fields influence magnetic anisotropy—one of the key levers to achieve ME coupling in molecular systems—by studying a complex with both a large axial ZFS and non-zero rhombicity. To this end, we investigate a system where the Mn(II) ($S$ = 5/2) magnetic center is replaced by a Ni(II) ($S$ = 1), *i.e.*, $[Ni(Me_6tren)Cl]^+$, hereafter referred to as complex **1**.[32] The high uniaxial ZFS ($D \approx -108$ cm$^{-1}$ at the optimized geometry) results from significant spin–orbit coupling. Jahn–Teller distortion contributes to substantial rhombicity, $E$, which was strictly zero for the Mn(II) complex that does not exhibit Jahn–Teller distortion. Enhanced spin–orbit coupling effects should lead to stronger electric-field sensitivity of the ZFS parameters.

The ME effect in this context is quantified through the variation of the ZFS parameters with the electric field strength $\vec{F}$, *i.e.*, d$D$/d$F$ and d$E$/d$F$. We also examine the field-orientation dependence of these parameters. Since the molecule possesses a dipole moment, applying the field along the dipole moment orientation is expected to strongly influence its geometry. Finally, following the same strategy as the one we used previously,[22] we decouple and quantify the impact of the electric field on the electronic structure and on the geometric structure.

A further motivation for selecting a Ni(II) complex lies in its integer spin ($S$ = 1) and a negative $D$ parameter, which allows the molecular geometry to give rise to two low-lying states (linear combinations of $M_S = \pm 1$) that may serve as a qubit at zero magnetic field, forming a so-called "clock transition." Clock transitions are known to protect spin states—at first order—from magnetic fluctuations that cause decoherence.[12,33–37] In such systems, electric fields can be used to tune the superposed quantum states. Understanding the electric field's influence on the rhombic ZFS parameter $E$ is therefore valuable for implementing single-qubit gates in these molecular systems.

## Theory and computational information

### Methodology for the rationalization of the nature and magnitude of ZFS for $[Ni(Me_6trenCl)](ClO_4)$ 1 upon electric field application

**1** crystallizes in the trigonal space group $R3c$, imposing a molecular three-fold symmetry axis $C_3$ along the Ni–Cl direction (Fig. 1a) and a $C_3$ symmetry point group.[32] However, some of us have already shown through both EPR studies and theoretical calculations that **1** is prone to a Jahn–Teller effect, which induces a distortion in the plane perpendicular to the Ni–Cl direction, leading to a $C_1$ symmetry point group. This effect lifts the degeneracy of the d orbitals (Fig. 1b) and hence of the spin–orbit-free states, responsible for the experimentally observed rhombicity ($E \neq 0$). Calculations of the energies of the spin–orbit-free states show an energy difference of 2166 cm$^{-1}$ between the ground $T^0$ and the first excited $T^1$ triplet states. Each of these two states is mainly spanned by a single determinant: $|d_{xz}\bar{d}_{xz}d_{yz}\bar{d}_{yz}d_{xy}\bar{d}_{xy}d_{x^2-y^2}d_{z^2}|$ (see Fig. 1b in $C_1$ symmetry) with a weight of 0.93 in $T^0$ and $|d_{xz}\bar{d}_{xz}d_{yz}\bar{d}_{yz}d_{xy}d_{x^2-y^2}\bar{d}_{x^2-y^2}d_{z^2}|$ (where an electron has been excited from $d_{xy}$ to $d_{x^2-y^2}$) with a weight of 0.98 in $T^1$. Therefore, the symmetry lowering due to the Jahn–Teller distortion leads to a situation where the spin is a not-too-bad quantum number. The ZFS spin Hamiltonian is,

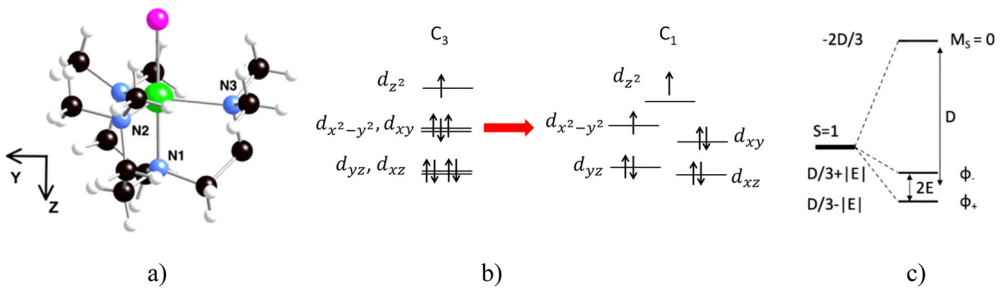


Fig. 1 (a) Representation of **1** with Ni in green, Cl in pink, N in blue, C in black, and H in white; (b) relative energy of the d orbitals of **1** in the case of a $C_3$ symmetry with the two couples of degenerate orbitals, and the main configuration in the $T^0$ ground state in the presence of a Jahn–Teller distortion inducing a $C_1$ symmetry; note the lift of degeneracy of the d orbitals; (c) the energy difference of the SO states ($M_S$ = 0) corresponds to $T^0_0$, while $\phi_+$ and $\phi_-$ are the + and − combinations of the $M_S$ = 1 ($T^0_{+1}$) and $M_S$ = −1 ($T^0_{-1}$) components of the ground state, as a function of the ZFS parameters $D$ and $E$.

 

hence, relevant to describe the energy of the spin states with the axial $D$ and the rhombic $E$ parameters of the **D** tensor (Fig. 1c). The easy axis of magnetization ($Z$) is along the pseudo $C_3$ axis and the $YZ$ plane contains the Ni–N3 bond (Fig. 1a).

In order to better understand the effect of an electric field, we use the strategy we had implemented in the study of the manganese complex.[22] This consists of decoupling and quantifying the impact of the field on the electronic structure (*i.e.*, effect of the electron cloud deformation) from that on the geometric structure. In case (a), the ZFS is calculated by applying the field on the geometry optimized without a field, which allows us to obtain the effect of the field on the electronic structure alone. In case (b), the ZFS is calculated without applying the field but on different geometries optimized under a field. The absence of the field removes the deformation of the electron cloud, allowing us to assess the impact of the field on the geometric structure alone. In case (c), the ZFS is calculated in the presence of the field on the geometries optimized under a field and therefore combines both effects.

The electric field is first applied along the Ni–Cl direction, *i.e.* along $Z$ that corresponds to the easy axis of magnetization and where the component of the dipole moment is maximal. To study the dependence of the ZFS parameters on the field orientation, we then apply the field along $Y$; the $YZ$ plane contains the N1, Ni and N3 atoms (Fig. 1a). The Ni–N3 bond length is the most different and shortest among the three Ni–N bonds in the $XY$ plane. To rationalize the field dependence of the ZFS parameters, we use a perturbative approach in order to account for the main variations in the contributions of the excited states. The SO Hamiltonian used for the rationalization is $H^{\mathrm{SOC}} = \sum_i \zeta\left(l^i_x s^i_x + l^i_y s^i_y + l^i_z s^i_z\right)$, where $i$ runs over all electrons of the $d^8$ configuration. As already shown,[32] the first excited triplet state has the largest (negative) contribution to $D$ and is responsible for its negative sign. This contribution is due to the interaction *via* SOC between, on the one hand, the two $M_S = 1$ and, on the other hand, the two $M_S = -1$ components of the ground state ($T^0_{\pm1}$) and the first excited state ($T^1_{\pm1}$) components. At the second order of perturbation, this contribution is given by eqn (1):

$$C(D)^{(2)}_{\mathrm{PERT.}} = -\frac{\left|\left\langle T^0_{\pm1}\middle|\middle|H^{\mathrm{SOC}}\middle|\middle|T^1_{\pm1}\right\rangle\right|^2}{\Delta E} \qquad (1)$$

where $\Delta E = E(T^1) - E(T^0)$ is the energy difference between the ground $T^0$ and first excited $T^1$ spin–orbit-free states. As the same $M_S$ components are involved in the bra and the ket, only the $l^i_z s^i_z$ part of the operator couples these components. This contribution stabilizes the largest $|M_S|$ values in comparison to the $T^0_0$ component and thus gives a negative value of $D$.

Of course, other excited triplet states, coupled through the $l^i_x s^i_x + l^i_y s^i_y$ part of the SOC operator, can bring positive contributions to $D$ by couplings their $M_S = \pm1$ components to the $M_S = 0$ ($T^0_0$) component of the ground state. The open-shell singlet $S^1$ based on the same electronic configuration as $T^1$ also couples through $l^i_z s^i_z$ to $T^0_0$, providing a positive contribution. These contributions must be taken into account in order to recover the correct value of $D$. However, the electric field has almost no impact on those terms (see Table S1); they are therefore not considered in the rationalization of the electric field effect. While eqn (1) is used to rationalize the results, more precise values of the contributions are provided by a procedure[38,39] based on the effective Hamiltonian theory,[40,41] which is implemented in the standard code ORCA (see the Computational information section).[42,43] We refer interested readers to the four previously cited articles.

If the $X$ and $Y$ axes of the molecular coordinates are those of the **D** tensor, the rhombic parameter $E$ comes from the effective coupling between the $M_S = 1$ and $-1$ components of the ground triplet state ($T^0_1$ and $T^0_{-1}$), which leads to two spin–orbit non-degenerate states that are linear combinations of these components. This effective coupling is due to the SOCs between these components and the excited states. The contributions of the excited states to the rhombic parameter $E$ are also provided by the code ORCA. Unfortunately, as this quantity is particularly small for **1**, the trends in $E$ as a function of the field are not always reproduced by the sum of the contributions of each excited state, which in some cases is even opposite to the variation in $E$. Therefore, we do not use these contributions for rationalization purposes. Instead, we use the analysis of the wave functions of the two excited states that contribute most to the rhombic parameter $E$ and give information on the difference in electron density in the $X$ and $Y$ directions, and therefore on the magnitude of $E$.

The field is applied in two opposite directions referred to as positive $+F$ and negative $-F$ with a maximal amplitude of $|F| = 1.028 \times 10^9$ V m$^{-1}$. The positive direction for the field in the $Z$ direction induces an elongation of the $Ni^{2+}$–$Cl^-$ bond, *i.e.*, the positive region of the electric potential is above $Cl^-$ in Fig. 1. The positive direction for the field in the $Y$ direction induces an elongation of the $Ni^{2+}$–$N_3$ bond, *i.e.*, the positive region of the electric potential is to the right of $N_3$ in Fig. 1a. One may note that, as is the case in other *ab initio* calculations of the impact of the electric field on electronic and/or magnetic properties,[22,29,31] the values of the field (that would be achievable by STM) are much greater than those used experimentally (in EPR experiments, for instance). As shown later, (i) geometric distortions are particularly small, so for the sake of precision, it is safer to apply strong fields, and (ii) the variations of the ZFS parameters with the field are linear and the slopes would be unchanged for lower values of the field.

## Computational information

Wave function-based calculations have been performed using the ORCA package.[42,43] In the first place, complete active space self-consistent field (CASSCF) calculations have been performed to account for non-dynamic correlations. The CAS(8,5) active space contains 8 electrons in the 5 orbitals mainly carried by the 3d orbitals of the Ni(II) ion, and the set of orbitals has been optimized using an average procedure over all triplet and all singlet states of the configuration. To account for dynamic correlations at the 2nd order of perturbation, NEVPT2[44] calculations have been carried out for all states. The spin–orbit state-interaction method[45] was then used to account for spin–orbit couplings (SOCs) between the $M_S$ components of all spin states

using the NEVPT2 correlated energies as diagonal elements of the SO matrix. The QZVPP extended basis sets[46] have been used for Ni atoms (14s10p5d4f2g), SVP for H (2s1p) and TZVP for all other atoms (6s3p2d1f for N, 8s4p2d1f for Cl and 6s3p2d1f for C). This approach has been successfully employed in numerous studies investigating the magnetic anisotropy of transition metal[47–57] and lanthanide and actinide[58–65] complexes.

As the field may change the geometric structure, geometry optimizations were performed for different values and orientations of the field.[42] We used the Hay–Wadt LanL2TZ(f) basis set[66,67] for Ni and its corresponding relativistic effective core, a Pople triple-ζ basis set (6-311G) for N[68] and Cl[69] atoms, a Pople double-ζ plus polarization basis set (6-31G*)[70] for C atoms, and a Pople double-ζ basis set (6-31G) for H atoms[70] and the B3LYP functional.[71] As magnetic anisotropy parameters may be very sensitive to the structure of the coordination sphere of the metal,[56,72] convergence thresholds for geometry optimization were set as VERYTIGHT. It should be noted that only geometry optimizations were performed at the DFT level; all values of magnetic anisotropy parameters were obtained at the CAS + NEVPT2 + SOSI level.

## Results and discussion

### Impact of the electric field on the axial ZFS parameter *D*

We begin by studying the impact of the electric field on the variation in the ground state energy illustrated in Fig. S1 and on the dipole moment presented in Table 1. The application of the field along the $Z$ direction from $-F$ to $+F$ leads globally to a linear variation of the energy of the ground state dominated by the electronic structure variation (case (a)) as expected for a Stark effect (Fig. S1). This linear behavior results from the fact that $\mu_Z$ is the largest component of the dipole moment so that the variation of the field does not cause a change of its sign (Table 1). The situation is different when the field is applied along the $Y$ direction. Here, the energy of the ground state has a global quadratic variation also dominated by the electronic structure variation (case (a); Fig. S1). The quadratic behavior stems from the change of the sign of $\mu_Y$ when the field is varied (Table 1), since $\mu_Y$ is almost zero (−0.054 Debye) for $F = 0$. It is worth noting that the overall variation of the dipole moment ($\Delta\mu_i$) has the same magnitude when $F$ is parallel or perpendicular to $Z$ (*i.e.* along the $Y$ direction) even though $\mu_Z$ is almost one order of magnitude larger than $\mu_Y$ for all field values.

Table 1 $Z$ and $Y$ components of the dipole moment in Debye and their variations between $-F$ and $+F$ values for the field applied along the $Z$ and $Y$ directions, respectively, for cases (a), (b) and (c). We may notice that the main contribution comes from the electronic structure changes, *i.e.*, the deformation of the electronic cloud, as cases (a) and (c) show very similar values

| | (a) | (b) | (c) |
|---|---|---|---|
| $\mu_Z$ at $-F$ | 7.19 | 8.04 | 7.13 |
| $\mu_Z$ at $+F$ | 9.02 | 8.17 | 9.08 |
| $\Delta\mu_Z$ | 1.83 | 0.13 | 1.95 |
| $\mu_Y$ at $-F$ | −0.97 | −0.12 | −1.03 |
| $\mu_Y$ at $+F$ | 0.86 | 0.01 | 0.93 |
| $\Delta\mu_Y$ | 1.83 | 0.13 | 1.96 |

The variation of $D$ with the field is linear in all three cases, whether the field is parallel or perpendicular to $Z$, as expected for non-centrosymmetric species (Fig. 2). The additivity of the slopes (Table 2) shows that our method of decomposition of the impact of the field on the electronic structure and geometry is reliable. Comparison of the results obtained for the three cases shows that the overall variation of $D$ (case (c)) is dominated by the impact of the field on the geometry (case (b)) for both directions of the field.

When $F//Z$ increases, $|D|$ increases with the change in electronic structure (case (a)), while it decreases in both cases (b) and (c). The situation is opposite when the field is perpendicular to $Z$ ($F//Y$), *i.e.*, $|D|$ decreases for a change in the electronic structure (case (a)), while it increases in both cases (b) and (c). More importantly, the variation of $|D|$ is almost 7 times larger when $F$ is along the $Y$ axis than when it is along the $Z$ axis, even though the dipole moment is one order of magnitude larger along the $Z$ axis than along the $Y$ axis.

To rationalize these results, we analyze the contribution $C(D)$ to $D$ from the most contributing excited states. The largest contribution is provided by the first excited triplet state $T^1$ (Tables S1 and S2) and this contribution is also the most sensitive to the field, *i.e.*, the variation $\Delta C(D)$ with the field

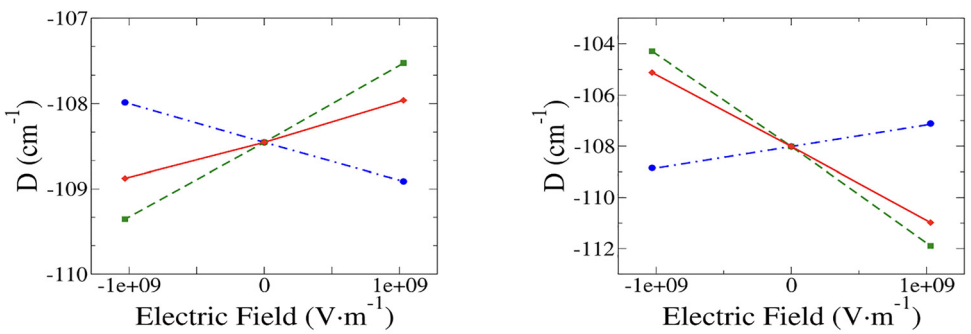


Fig. 2 Axial parameter $D$ as a function of the field applied in the $Z$ (left) and $Y$ (right) directions. Case (a): electronic effect only (blue dot-dashed line), case (b): geometric effect only (green dashed line) and case (c): both electronic and geometric effects (red solid line).

 

Table 2 Slopes ($dD/dF$ in Hz/(V m$^{-1}$)) of the straight lines in cases (a), (b), and (c) for the variation of the parameter $D$ with the electric field oriented along the $Z$ and $Y$ directions

| Hz/(V m$^{-1}$) | Case (a) | Case (b) | Case (c) | Sum of cases (a) and (b) |
|---|---|---|---|---|
| $dD/dF$ ($F//Z$) | −13.52 | +26.66 | +13.15 | +13.14 |
| $dD/dF$ ($F//Y$) | 25.32 | −110.75 | −85.45 | −85.43 |

Table 3 Variations $\Delta C(D)$ of the contributions to the axial parameter $D$ of the first excited state $T^1$, $\Delta(\Delta E)$ is the variation of its energy difference to the ground state and $\Delta(\Delta\varepsilon(d_{x^2-y^2} - d_{xy}))$ is the variation of the energy difference between the $d_{x^2-y^2}$ and $d_{xy}$ orbitals. All variations are calculated between $-F$ and $+F$ along the $Z$ axis ($F//Z$) and the $Y$ axis ($F//Y$) and are given in cm$^{-1}$

| Orientation of $F$ for cases (a), (b) and (c) | | $\Delta C(D)$ | $\Delta(\Delta E)$ | $\Delta(\Delta\varepsilon(d_{x^2-y^2} - d_{xy}))$ |
|---|---|---|---|---|
| $F//Z$ | (a) | −0.88 | −1.60 | 6.58 |
| | (b) | 2.70 | 36.2 | 258.98 |
| | (c) | 1.83 | 34.7 | 267.76 |
| $F//Y$ | (a) | 1.73 | 24.40 | 274.34 |
| | (b) | −8.84 | −122.40 | −561.86 |
| | (c) | −7.11 | −98.20 | −287.51 |

has by far the highest value. Therefore, only the properties of $T^1$ are reported in Table 3. It is worth noting that the variations with the field (Tables S1 and S2) of the contributions calculated perturbatively $C(D)^{(2)}_{\text{PERT.}}$ (eqn (1)) are in good agreement with those calculated *ab initio*, showing that one may use the variation of the energy differences between the spin–orbit free states to rationalize the impact of the field on the parameter $D$. In the following, we consider the variation of the absolute value of $D$ ($|D|$) when the field is varied from $-F$ to $+F$.

**Field applied along the *Z* axis (*F*//*Z*).** In case (a), the energy difference between the ground state and $T^1$ (see $\Delta(\Delta E)$ in Table 3) slightly decreases. This variation is so small that we also analyze the evolution of the SOC (see Table S1), which increases. Both factors are compatible with a negative sign of $dD/dF$, *i.e.* an increase of $|D|$ (see the SI for the rationalization of the increase in the SOC). In contrast, in cases (b) and (c), $\Delta E$ increases. These results are consistent, according to eqn (1), with a decrease of $|D|$ in cases (b) and (c). The overall variation (case (c)) is a decrease of $|D|$ since the effect of the change in the geometric structure (case (b)) is predominant. It is therefore possible to rationalize the variation in energy differences $\Delta(\Delta E)$ using the impact of the geometric changes on the ligand field.

The energy difference $\Delta E$ between the ground state and $T^1$ is mainly governed by the energy difference $\Delta\varepsilon(d_{x^2-y^2} - d_{xy})$ between the $d_{x^2-y^2}$ and $d_{xy}$ orbitals because $T^1$ is obtained following an excitation from $d_{xy}$ to $d_{x^2-y^2}$ (Fig. 1). Table 3 also shows the variation $\Delta(\Delta\varepsilon(d_{x^2-y^2} - d_{xy}))$ of these energy differences between $-F$ and $+F$. They can be directly linked to the change in the ligand field under the effect of the electric field. Indeed, for $+F$, the Ni–Cl bond length increases (Table 4) in order to maximize the dipole moment and thus the interaction with the electric field. Concomitantly, all the other distances

Table 4 Variations of the distance ($\Delta(d)$ in Angstrom) in the coordination sphere of Ni(II) between $-F$ and $+F$ along the $Z$ and $Y$ axes

| $d$(Ni–X) | $\Delta(d)$, $F//Z$ | $\Delta(d)$, $F//Y$ |
|---|---|---|
| Cl | $131.8 \times 10^{-4}$ | $2.4 \times 10^{-4}$ |
| N1 (apical) | $-28.9 \times 10^{-4}$ | $1.7 \times 10^{-4}$ |
| N2 | $-69.6 \times 10^{-4}$ | $-27.3 \times 10^{-4}$ |
| N3 | $-48.9 \times 10^{-4}$ | $11.4 \times 10^{-4}$ |
| N4 | $-66.5 \times 10^{-4}$ | $-4.1 \times 10^{-4}$ |

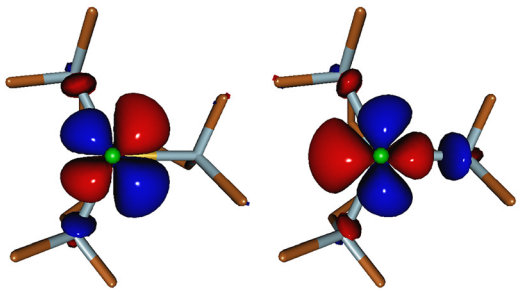

Fig. 3 Picture of the $d_{xy}$ (left) and $d_{x^2-y^2}$ (right) orbitals optimized at the CASSCF level in the absence of a field.

decrease, inducing a stronger ligand field in the $X$ and $Y$ directions, which affects the energy of the $d_{x^2-y^2}$ orbital directly pointing towards the N3 atoms (see Fig. 3) more than that of $d_{xy}$. The energy difference between these two orbitals therefore increases with the field, resulting in a greater energy difference between the ground state and the first excited state, responsible for the decrease in $|D|$, according to eqn (1).

**Field applied along the *Y* axis (*F*//*Y*).** Similar to when the field is applied along the $Z$ axis, here as well we can relate the variation in the contribution to $D$ to the energy difference between the ground state and $T^1$, *i.e.*, $|D|$ decreases (case (a)) or increases (cases (b) and (c)) when the energy difference varies inversely, as expected from eqn (1). Similarly, the energy difference between the states can be correlated with the energy difference between the $d_{x^2-y^2}$ and $d_{xy}$ orbitals. Thus, here again, the variation of $D$ can be rationalized by the change in the ligand field due to the geometric distortions induced by the electric field.

The application of the field along the $Y$ axis leads to an increase of the Ni–N3 bond length and to a decrease of the two other Ni–N distances in the $XY$ plane (Table 3). These geometric changes result in a weaker ligand field in the $Y$ direction and a stronger ligand field between the $X$ and $Y$ axes. The tails of the $d_{x^2-y^2}$ and $d_{xy}$ orbitals on the ligands (Fig. 3) illustrate the delocalization of $d_{x^2-y^2}$ mainly on N3, while $d_{xy}$ delocalizes on N2 and N4. Consequently, the $d_{x^2-y^2}$ orbital is stabilized, while $d_{xy}$ is destabilized, leading to a decrease of the energy difference $\Delta\varepsilon$ between the two orbitals and therefore a decrease of the energy difference $\Delta E$ between the ground and the first excited state. According to eqn (1), this rationalizes the increase of $|D|$ (Table 3).

The principal conclusion drawn from the above studies and their analysis is that the electric field exerts a stronger influence

on $D$ when applied along the $Y$ direction, which is perpendicular to the largest dipole moment. This behavior, which is in contrast to previously reported experimental observations and theoretical predictions,[17,18,20,22] stems from the nature of the excitation responsible for the strong contribution to $D$. Indeed, the energy of the excitation from $d_{xy}$ to $d_{x^2-y^2}$ is much more sensitive to a perturbation applied along the $Y$ than along the $Z$ axis, rationalizing the stronger response when the field is perpendicular to the largest dipole moment.

### Impact of the electric field on the rhombic term $E$

The variation of $E$ with the field is linear in all three cases, whether the field is parallel or perpendicular to the $Z$ axis (Fig. 4); however, due to a lack of precision in calculating this particularly small quantity, the coefficient of trend line determination for case (b) and $F//Z$ is lower (0.88) than that of all others ($>0.99$). Here again the additivity of the slopes (Table 5) demonstrates the accuracy of our method of decomposition. Comparison of the results obtained for the three cases shows that the overall variation of $E$ (case (c)) is dominated by the impact of the field on the electronic structure (case (a)) for both directions of the field.

When $F//Z$ increases, $E$ decreases in cases (a) and (c), while it remains almost constant in case (b). The situation is similar for cases (a) and (c) when the field is perpendicular to $Z$ ($F//Y$), but it now increases in case (b). It can also be noted that the strongest response to the field is now obtained for the direction $F//Z$.

Unfortunately, it was not possible to use the contributions to $E$ calculated *ab initio* to rationalize the obtained results. Indeed, the sum of the contributions increases with the field, while the overall computed values of $E$ decrease. Nevertheless, it is possible to analyze the wave functions of the third and fourth triplet states $T^2$ and $T^3$ that contribute mostly to $E$, with contributions of opposite sign. The wave functions of these states have large coefficients on the determinants with three electrons in the pair of orbitals $d_{xz}$ and $d_{yz}$, *i.e.* resulting from single excitations (from $T^0$) from the $d_{xz}$ or $d_{yz}$ orbital to either $d_{x^2-y^2}$ or $d_{z^2}$ (see Fig. 1c). Since $d_{x^2-y^2}$, $d_{xy}$ and $d_{z^2}$ are symmetric in the $X$ and $Y$ directions, only six determinants with $M_S = 1$ distinguish the $X$ and $Y$ axes: three have a single occupation in $d_{xz}$ and the other three have a single occupation in $d_{yz}$. In the case of purely axial anisotropy, *i.e.* $E = 0$, we can expect the weights of the first three determinants to be equal to those of the last three ones in $T^2$ and $T^3$, ensuring equal electron density in the $X$ and $Y$ directions and therefore strictly offsetting contributions. The weights $w(d_{xz})$ and $w(d_{yz})$ of determinants having a single occupation in $d_{xz}$ or $d_{yz}$, respectively, their differences $\Delta w(X - Y)$ and the variations of their difference $\Delta(\Delta w(Y - X))$ between $-F$ and $+F$ are reported in Table S3. Only the variations of their differences are reported in Table 6.

Table 5 Slopes ($dE/dF$ in Hz/(V m$^{-1}$)) of the straight lines in cases (a), (b), and (c) for the variation of the parameter $E$ with the electric field oriented along the $Z$ and $Y$ axes

| Hz/(V m$^{-1}$) | Case (a) | Case (b) | Case (c) | Sum of cases (a) and (b) |
|---|---|---|---|---|
| $dE/dF$ ($F//Z$) | −2.53 | −0.36 | −2.88 | −2.89 |
| $dE/dF$ ($F//Y$) | −2.39 | 1.20 | −1.19 | −1.19 |

**Field applied along $Z$ ($F//Z$).** We observe that the difference $\Delta w(X - Y)$ (Table S3) of the weights between $X$ and $Y$ decreases with the field, indicating that the field diminishes the rhombicity. We can also note that these changes are negligible for case (b), whereas they are almost identical for case (a) and case (c), rationalizing the fact that changes in the electronic structure are the dominant effect of the variation with the field of the rhombic parameter $E$.

**Field applied along $Y$ ($F//Y$).** Here again the difference $\Delta w(X - Y)$ of the weights between $X$ and $Y$ decreases with the field in cases (a) and (c) in agreement with the negative slopes of $E$ *versus* field in Fig. 4. We can also observe that these weight differences slightly increase for case (b) (geometric contributions), which is consistent with the increase of rhombicity (positive slope) in this particular case.

The strongest response of the rhombic parameter $E$ to the electric field is observed when it is applied in the $Z$ direction. This result is here as well determined by the nature of the excitations providing the main contributions to $E$. Indeed, in the two states $T^2$ and $T^3$, the orbitals, namely $d_{xz}$ or $d_{yz}$, involved in the excitation have a component along the $Z$ axis. Hence, the corresponding excitation energies will be more sensitive to a perturbation applied in the $Z$ than along the $Y$ direction.

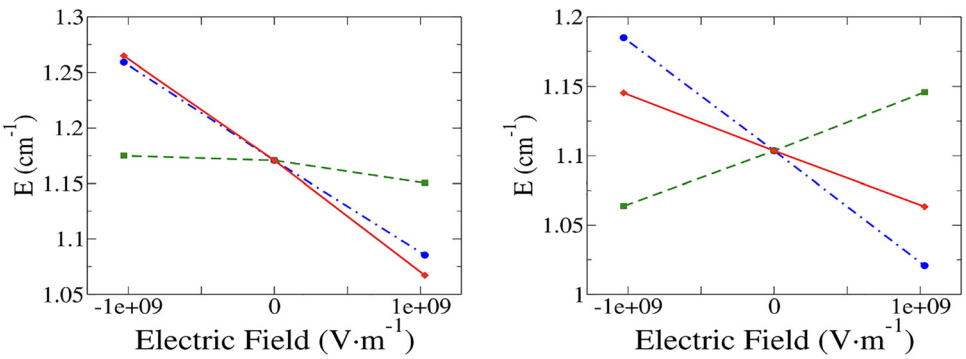


Fig. 4 Rhombic parameter $E$ as a function of the field applied in the $Z$ (left) and $Y$ (right) directions. Case (a): electronic effect only (blue dot-dashed line), case (b): geometric effect only (green dashed line) and case (c): both electronic and geometric effects (red solid line).

 

Table 6 Variations $\Delta(\Delta w(Y-X))$ (see text) of the difference of the weights of the determinants having a single occupation either in the $d_{xz}$ or in the $d_{yz}$ orbital between the $-F$ and $+F$ values of the field applied along the $Z$ and $Y$ axes

| | $F//Z$ | $F//Y$ |
|---|---|---|
| Case (a) | −0.528 | −0.174 |
| Case (b) | −0.088 | +0.002 |
| Case (c) | −0.621 | −0.170 |

## Conclusions

Through an accurate decomposition of the impact of the electric field on the electronic and geometric structures, it has been possible to provide an in-depth analysis of the effect of the electric field on ZFS parameters. The main results can be summarized as follows:

(i) The variation in $D$ caused by the impact of the field on the electronic structure alone (case (a)) is opposite to that induced by geometric changes (case (b)). When both electronic and geometric changes are accounted for in the calculation (case (c)), a similar behavior to that in case (b) is observed, showing that the impact of the field on the axial parameter in mainly governed by the field-induced geometric changes. It is true for both directions of the application of the field: for $F//Z$, $|D|$ decreases, while it increases for $F//Y$. As the geometric changes dominate the response of $D$ to the field, an analysis of the ligand field changes induced by the field can be used to rationalize both results.

(ii) Concerning the rhombicity $E$, we observe that the overall (case (c)) response to the electric field is dominated by the electronic structure changes (case (a)). To rationalize these results, we analyzed the wave functions of the excited states contributing most to $E$.

The most spectacular and interesting result is the variation of the axial parameter $D$ with the field that is considerably $\sim$100 times greater than that observed in our previous study on $[Mn(Me_6tren)X]^+$. More importantly, $d|D|/dF$ is $\sim$7 times larger when the field is applied along the direction where the dipole moment component $Y$ is very small than along the $Z$ direction where it is close to 10 Debye. The variation of the parameter $E$ is less important but still large in particular for $F//Z$. As $E$ quantifies the anisotropy between $X$ and $Y$, one might have expected that applying the field along the $Y$ axis would generate greater effects than along the $Z$ axis. Actually, these *a priori* non-intuitive results are rationalized by the nature of the excitations involved in the SOCs that generate the magnetic anisotropy. Indeed, in the case of the axial parameter $D$, the first excited $T^1$ state, which provides the most significant and sensitive contribution to the field, results from the excitation from $d_{xy}$ to $d_{x^2-y^2}$. The energy difference between these two orbitals is less affected by the application of the field along the $Z$ than the $Y$ axis, which clearly discriminates the two orbitals as $d_{x^2-y^2}$ directly points toward the $Y$ axis. The same conclusion is reached when rationalizing the response to the field of the parameter $E$. The most important contributions to $E$ come from the $T^2$ and $T^3$ excited states, which are coupled to the ground state by excitations from $d_{xz}$ or $d_{yz}$ to the $d_{z^2}$ or $d_{x^2-y^2}$ orbital, involving mainly d orbitals with a $Z$ component. It is therefore natural for these excitations to be more sensitive to the field along the $Z$ direction than along the $Y$ direction.

Although our study of the $[MnMe_6trenCl]^+$ complex[22] concluded that the strongest electric-field response of $D$ occurs when the field is applied collinearly with the dipole moment, these new results do not contradict that conclusion. In the Mn(II) system, the $d^5$ electronic configuration gives rise to numerous excitations involving all d orbitals, each contributing weakly and often with opposite signs to the axial parameter $D$. Therefore, no clear conclusion regarding the role of excitation character could be drawn. Instead, geometric distortions—enhanced when the field is applied along the dipole moment—dominate the electric-field dependence of $D$. In contrast, the present results demonstrate that the dominant factor can be the nature of the orbitals involved in the relevant electronic excitations. The conclusions of both studies suggest a general design principle for maximizing electric-field responses: when one of the two orbitals involved in a key excitation is aligned with the dominant dipole component, the excitation energy becomes particularly sensitive to the applied field, leading to an enhanced response of the ZFS parameters.

The main message of this work is that the magnetoelectric effect—expressed here as a change in the ZFS parameters, *i.e.* the slopes $dD/dF$ and $dE/dF$—can be very large. The modulation of the magnetic properties by the electric field is not necessarily large only when the field is oriented in the direction of the dipole moment. For both $D$ and $E$, the nature of the excitations that couple the ground state to the various excited states responsible for the strongest contributions is the determining factor. Finally, we have shown that most of the rationalization of these effects requires analysis of the impact of the field on the orbitals involved in these excitations and can be related to ligand field theory. These conclusions, even though they were highlighted in a specific case, are general in nature, which is promising for the design of new complexes whose magnetic properties can be controlled and tuned by the electric field. Finally, the predicted large change in the ZFS parameters ($dD/dF$ and $dE/dF$) can be useful for technological applications in the sense that weak electric fields may induce detectable magnetoelectric effects.

## Conflicts of interest

There are no conflicts to declare.

## Data availability

The data that support the findings of this study are available from the authors upon request.

Supplementary information (SI) is available. See DOI: https://doi.org/10.1039/d5cp03260a.

## Acknowledgements

N. G., N. S. and T. M. thank the ANR for financial support through project ANR-20-CE29-0010. This work also received government funding managed by the French National Research Agency under France 2030, reference ANR-23-PETQ-0007.

## References

1 R. Ramesh and S. Manipatruni, *Proc. R. Soc. A*, 2021, **477**, 20200942.
2 J. Long, M. S. Ivanov, V. A. Khomchenko, E. Mamontova, J.-M. Thibaud, J. Rouquette, M. Beaudhuin, D. Granier, R. A. S. Ferreira, L. D. Carlos, B. Donnadieu, M. S. C. Henriques, J. A. Paixão, Y. Guari and J. Larionova, *Science*, 2020, **367**, 671–676.
3 Y.-X. Wang, D. Su, Y. Ma, Y. Sun and P. Cheng, *Nat. Commun.*, 2023, **14**, 7901.
4 J. Liu, J. Mrozek, W. K. Myers, G. A. Timco, R. E. P. Winpenny, B. Kintzel, W. Plass and A. Ardavan, *Phys. Rev. Lett.*, 2019, **122**, 037202.
5 A. K. Boudalis, J. Robert and P. Turek, *Chem. – Eur. J.*, 2018, **24**, 14896–14900.
6 M. Lewkowitz, J. Adams, N. S. Sullivan, P. Wang, M. Shatruk, V. Zapf and A. S. Arvij, *Sci. Rep.*, 2023, **13**, 2769.
7 N. Guihery, G. Durand, M.-B. Lepetit and J.-P. Malrieu, *Chem. Phys.*, 1994, **183**, 61–72.
8 B. E. Kane, *Nature*, 1998, **393**, 133–137.
9 A. S. Zyazin, J. W. G. van den Berg, E. A. Osorio, H. S. J. van der Zant, N. P. Konstantinidis, M. Leijnse, M. R. Wegewijs, F. May, W. Hofstetter, C. Danieli and A. Cornia, *Nano Lett.*, 2010, **10**, 3307–3311.
10 B. Kintzel, M. Fittipaldi, M. Böhme, A. Cini, L. Tesi, A. Buchholz, R. Sessoli and W. Plass, *Angew. Chem., Int. Ed.*, 2021, **60**, 8832–8838.
11 Z. Liu, Y.-X. Wang, Y.-H. Fang, S.-X. Qin, Z.-M. Wang, S.-D. Jiang and S. Gao, *Natl. Sci. Rev.*, 2020, **7**, 1557–1563.
12 J. Liu, J. Mrozek, A. Ullah, Y. Duan, J. J. Baldoví, E. Coronado, A. Gaita-Ariño and A. Ardavan, *Nat. Phys.*, 2021, **17**, 1205–1209.
13 L. Tacconi, A. Cini, A. Raza, L. Tesi, P. Bartolini, A. Taschin, J. van Slageren, M. Briganti, L. Sorace, M. Fittipaldi and M. Perfetti, *J. Am. Chem. Soc.*, 2025, **147**, 33040–33051.
14 S. Thiele, F. Balestro, R. Ballou, S. Klyatskaya, M. Ruben and W. Wernsdorfer, *Science*, 2014, **344**, 1135–1138.
15 M. Fittipaldi, A. Cini, G. Annino, A. Vindigni, A. Caneschi and R. Sessoli, *Nat. Mater.*, 2019, **18**, 329–334.
16 A. Cini, M. Böhme, B. Kintzel, M. Perfetti, W. Plass, R. Sessoli and M. Fittipaldi, *Nat. Commun.*, 2025, **16**, 6564.
17 R. E. George, J. P. Edwards and A. Ardavan, *Phys. Rev. Lett.*, 2013, **110**, 027601.
18 J. Liu, V. V. Laguta, K. Inzani, W. Huang, S. Das, R. Chatterjee, E. Sheridan, S. M. Griffin, A. Ardavan and R. Ramesh, *Sci. Adv.*, 2021, **7**, eabf8103.
19 Y.-H. Fang, Z. Liu, S. Zhou, P.-X. Fu, Y.-X. Wang, Z.-Y. Wang, Z.-M. Wang, S. Gao and S.-D. Jiang, *J. Am. Chem. Soc.*, 2022, **144**, 8605–8612.
20 Y.-C. Liu, J.-X. Chen, P.-X. Fu, Y.-Q. Liao, Y.-H. Wang, Y.-X. Wang, Z. Liu, S. Gao and S.-D. Jiang, *J. Am. Chem. Soc.*, 2024, **146**, 19397–19404.
21 Y.-C. Liu, J.-X. Chen, J.-F. Bu, P.-X. Fu, Y.-X. Wang, Z. Liu, S. Gao and S.-D. Jiang, *J. Am. Chem. Soc.*, 2025, **147**, 10423–10429.
22 M. V. Vaganov, N. Suaud, F. Lambert, B. Cahier, C. Herrero, R. Guillot, A.-L. Barra, N. Guihéry, T. Mallah, A. Ardavan and J. Liu, *Nat. Chem.*, 2025, **17**, 1903–1909.
23 B. Pradines, B. Cahier, N. Suaud and N. Guihéry, *J. Chem. Phys.*, 2022, **157**, 204308.
24 F. Meier, J. Levy and D. Loss, *Phys. Rev. Lett.*, 2003, **90**, 047901.
25 F. Troiani, *Phys. Rev. B*, 2019, **100**, 155424.
26 A. Sarkar and G. Rajaraman, *Chem. Sci.*, 2020, **11**, 10324–10330.
27 F. Heully-Alary, B. Pradines, N. Suaud and N. Guihéry, *J. Chem. Phys.*, 2024, **161**, 054310.
28 Y. Lu, Y. Wang, L. Zhu, L. Yang and L. Wang, *Phys. Rev. B*, 2022, **106**, 064405.
29 T. Sharma, A. Singh and G. Rajaraman, *Chem. – Eur. J.*, 2025, **31**, e202402868.
30 M. Trif, F. Troiani, D. Stepanenko and D. Loss, *Phys. Rev. B: Condens. Matter Mater. Phys.*, 2010, **82**, 045429.
31 W. T. Morrillo, H. I. J. Cumming, A. Mattioni, J. K. Staab and N. F. Chilton, *J. Am. Chem. Soc.*, 2024, **146**, 25841–25851.
32 R. Ruamps, R. Maurice, L. Batchelor, M. Boggio-Pasqua, R. Guillot, A. L. Barra, J. Liu, E.-E. Bendeif, S. Pillet, S. Hill, T. Mallah and N. Guihéry, *J. Am. Chem. Soc.*, 2013, **135**, 3017–3026.
33 M. Shiddiq, D. Komijani, Y. Duan, A. Gaita-Ariño, E. Coronado and S. Hill, *Nature*, 2016, **531**, 348–351.
34 S. Giménez-Santamarina, S. Cardona-Serra, J. M. Clemente-Juan, A. Gaita-Ariño and E. Coronado, *Chem. Sci.*, 2020, **11**, 10718–10728.
35 I. Tlemsani, F. Lambert, N. Suaud, C. Herrero, R. Guillot, A.-L. Barra, S. Gambarelli and T. Mallah, *J. Am. Chem. Soc.*, 2025, **147**, 4685–4688.
36 G. Chen, B. C. Sheehan, I. Nikolov, J. W. Logan, C. A. Collett, G. Joshi, G. A. Timco, J. E. Denhardt, K. R. Kittilstved, R. E. P. Winpenny and J. R. Friedman, *arXiv*, 2025, preprint, arXiv:arXiv:2507.13714, DOI: 10.48550/arXiv.2507.13714.
37 G. Wolfowicz, A. M. Tyryshkin, R. E. George, H. Riemann, N. V. Abrosimov, P. Becker, H.-J. Pohl, M. L. W. Thewalt, S. A. Lyon and J. J. L. Morton, *Nat. Nanotechnol.*, 2013, **8**, 561–564.
38 R. Maurice, R. Bastardis, C. de Graaf, N. Suaud, T. Mallah and N. Guihéry, *J. Chem. Theory Comput.*, 2009, **5**, 2977–2984.
39 J. P. Malrieu, R. Caballol, C. J. Calzado, C. de Graaf and N. Guihéry, *Chem. Rev.*, 2014, **114**, 429–492.
40 C. Bloch, *Nucl. Phys.*, 1958, **6**, 329–347.
41 J. des Cloizeaux, *Nucl. Phys.*, 1960, **20**, 321–346.
42 F. Neese, F. Wennmohs, U. Becker and C. Riplinger, *J. Chem. Phys.*, 2020, **152**, 224108.
43 F. Neese, *Wiley Interdiscip. Rev.: Comput. Mol. Sci.*, 2022, **12**, e1606.
44 C. Angeli, R. Cimiraglia, S. Evangelisti, T. Leininger and J.-P. Malrieu, *J. Chem. Phys.*, 2001, **114**, 10252–10264.

 

45 P. Å. Malmqvist, B. O. Roos and B. Schimmelpfennig, *Chem. Phys. Lett.*, 2002, **357**, 230–240.
46 F. Weigend and R. Ahlrichs, *Phys. Chem. Chem. Phys.*, 2005, **7**, 3297–3305.
47 Pentagonal Bipyramidal First-Row Transition Metal Complexes with Macrocyclic Ligand Containing Two Pyridine-N-Oxide Pendant Arms, https://colab.ws/articles/10.1021%2Facs.inorgchem.5c03514, (accessed December 17, 2025).
48 M. Malik, A. Bieńko, R. Boča, J. Titiš, C. Rajnák, A. Świtlicka, D. C. Bieńko, M. Ozerov and A. Ozarowski, *Dalton Trans.*, 2025, **54**, 16955–16965.
49 K. Bretosh, V. Béreau, F. Heully-Alary, N. Suaud, C. Duhayon, E. Duverger-Nédellec, N. Guihéry and J.-P. Sutter, *Inorg. Chem. Front.*, 2025, **12**, 3456–3468.
50 A. Colin, Y. Wang, F. Lambert, N. Bridonneau, N. Suaud, R. Guillot, E. Rivière, Z. Halime, N. Guihéry, S. Ohkoshi and T. Mallah, *Magnetochemistry*, 2024, **10**, 102.
51 A. Mukhopadhyaya and Md. E. Ali, *J. Phys. Chem. A*, 2024, **128**, 2339–2348.
52 D.-C. Sergentu, B. L. Guennic and R. Maurice, *Phys. Chem. Chem. Phys.*, 2024, **26**, 6844–6861.
53 J. Titiš, C. Rajnák and R. Boča, *J. Phys. Chem. A*, 2023, **127**, 6412–6424.
54 S. K. Gupta, S. V. Rao, S. Demeshko, S. Dechert, E. Bill, M. Atanasov, F. Neese and F. Meyer, *Chem. Sci.*, 2023, **14**, 6355–6374.
55 M. Atanasov, N. Spiller and F. Neese, *Phys. Chem. Chem. Phys.*, 2022, **24**, 20760–20775.
56 S. R. Chowdhury and S. Mishra, *Phys. Chem. Chem. Phys.*, 2017, **19**, 16914–16922.
57 R. Maurice, K. Sivalingam, D. Ganyushin, N. Guihéry, C. de Graaf and F. Neese, *Inorg. Chem.*, 2011, **50**, 6229–6236.
58 Y. Ai, Z.-W. Li, Z.-B. Guan and H. Jiang, *J. Chem. Theory Comput.*, 2025, **21**, 9631–9640.
59 Md. A. Islam, C. Berthon, J. Jung and H. Bolvin, *Inorg. Chem.*, 2023, **62**, 17254–17264.
60 A. B. Canaj, M. K. Singh, C. Wilson, G. Rajaraman and M. Murrie, *Chem. Commun.*, 2018, **54**, 8273–8276.
61 M. Perfetti, M. Gysler, Y. Rechkemmer-Patalen, P. Zhang, H. Taştan, F. Fischer, J. Netz, W. Frey, L. W. Zimmermann, T. Schleid, M. Hakl, M. Orlita, L. Ungur, L. Chibotaru, T. Brock-Nannestad, S. Piligkos and J. van Slageren, *Chem. Sci.*, 2019, **10**, 2101–2110.
62 M. Vonci, K. Mason, E. A. Suturina, A. T. Frawley, S. G. Worswick, I. Kuprov, D. Parker, E. J. L. McInnes and N. F. Chilton, *J. Am. Chem. Soc.*, 2017, **139**, 14166–14172.
63 B. Hong, A. Näder, T. Sawallisch, T. Bode, S. Fichter, R. Gericke, P. Kaden, M. Patzschke, T. Stumpf, M. Schmidt and J. März, *Inorg. Chem.*, 2024, **63**, 17488–17501.
64 S. Dey, G. Rajaraman and H. Bolvin, *Chem. – Eur. J.*, 2022, **28**, e202201883.
65 F. Gendron and J. Autschbach, *J. Phys. Chem. Lett.*, 2017, **8**, 673–678.
66 P. J. Hay and W. R. Wadt, *J. Chem. Phys.*, 1985, **82**, 299–310.
67 L. E. Roy, P. J. Hay and R. L. Martin, *J. Chem. Theory Comput.*, 2008, **4**, 1029–1031.
68 R. Krishnan, J. S. Binkley, R. Seeger and J. A. Pople, *J. Chem. Phys.*, 1980, **72**, 650–654.
69 A. D. McLean and G. S. Chandler, *J. Chem. Phys.*, 1980, **72**, 5639–5648.
70 W. J. Hehre, R. Ditchfield and J. A. Pople, *J. Chem. Phys.*, 1972, **56**, 2257–2261.
71 D. G. A. Smith, L. A. Burns, K. Patkowski and C. D. Sherrill, *J. Phys. Chem. Lett.*, 2016, **7**, 2197–2203.
72 P. A. Brayshaw, J.-C. G. Buenzli, P. Froidevaux, J. M. Harrowfield, Y. Kim and A. N. Sobolev, *Inorg. Chem.*, 1995, **34**, 2068–2076.